Turkish Journal of Physics

Volume 44 | Number 6 Article 4

1-1-2020

Tuning the magnetic field sensitivity of planar Hall effect sensors by using a Cr spacer layer in a NiFe/Cr/IrMn trilayer structure

HASAN PİŞKİN

NUMAN AKDOĞAN

TÜBİTAK

Turkish Journal of Physics

http://journals.tubitak.gov.tr/physics/

Research Article

Turk J Phys
(2020) 44: 554 – 563

doi:10.3906/fiz-2008-19

Tuning the magnetic field sensitivity of planar Hall effect sensors by using a Cr spacer layer in a NiFe/Cr/IrMn trilayer structure

Hasan PİŞKİN* , **Numan AKDOĞAN**
Department of Physics, Faculty of Science, Gebze Technical University, Gebze, Turkey

Received: 29.08.2020 • **Accepted/Published Online:** 10.11.2020 • **Final Version:** 18.12.2020

Abstract: Planar Hall effect (PHE)-based magnetic field sensors have recently received considerable attention due to their fascinating properties. For the NiFe/spacer/IrMn trilayer PHE sensor structures, tuning the exchange bias via a spacer layer is very crucial due to its direct effects on the sensor's magnetic field sensitivity. Here the effect of Cr spacer layer thickness on PHE sensitivity and exchange bias is investigated in NiFe (10 nm)/Cr (t_{Cr})/IrMn (20 nm) trilayer structures where the t_{Cr} varied between 0.0 nm and 1 nm with a step of 0.1 nm. As the t_{Cr} increased, we observed a fast decrease in exchange bias field. When the thickness of Cr spacer layer increased up to 0.7 nm, a maximum sensitivity of 4.4 μV/(Oe·mA) was obtained. Besides, sensor voltage exhibited ±100 nV noise level. With this noise level, a 1.6 μT magnetic field resolution was achieved.

Key words: Planar Hall effect, magnetoresistive sensors, exchange bias

1. Introduction

Nowadays, on-chip devices that can detect ultralow magnetic fields are gaining importance due to their potential applications such as magnetic bead/label sensing in bio-material detection [1–3], positioning sensors [4], tactile sensing [5], electronic compasses [6], and detection of microcracks in metallic shells [7]. For these applications, portability, small footprint, low power consumption, and cost-effectiveness are the key factors. Among the magnetoresistance (MR)-based magnetic field sensors, the planar Hall effect (PHE) sensors have the advantages such as easy fabrication, linear responses at low magnetic fields, high signal-to-noise ratios, bipolarity, and insensitiveness to small thermal fluctuations.

Recent studies on PHE sensors have focused on increasing/optimizing their magnetic field sensitivity and resolution either by changing sensor structure or its geometry [8–12]. In the literature, several types of exchange-biased sensor structures have already been studied such as NiFe/IrMn bilayers [13–15], NiFe/X/IrMn (X: Cu, Au, Pt) trilayers [8,12,16], and NiFe/Cu/NiFe/IrMn spin-valves [17,18]. It is found that the trilayer structures provide the highest sensor sensitivities due to their lower exchange bias (EB) and lower shunt currents compared to bilayers and spin-valves [8]. Besides, the type of nonmagnetic (NM) spacer layer inserted between NiFe and IrMn in a trilayer structure plays a crucial role in tuning the EB and shunt currents [12]. For example, although the insertion of Cu layer increases the sensitivity (by decreasing the EB), as the thickness of Cu layer is increased, a significant decrease can be observed in the sensor's output voltage due to the good conductivity of Cu [8]. The large decrease in the sensor's output voltage limits the sensor sensitivity even when the EB

*Correspondence: hasan.piskin@boun.edu.tr
Current address: Department of Physics, Faculty of Arts and Sciences, Boğaziçi University, İstanbul, Turkey

decreases. However, when the Au and Pt spacer layers are used instead of Cu, a remarkable increase in sensor's output voltage is observed despite the increased shunt currents [12,16]. These findings show that the proper choice of spacer layer is very important for designing a PHE-based sensor.

Here we expand the literature data by inserting a Cr spacer layer between NiFe and IrMn in traditional cross-junction geometry of PHE sensors. The Cr material has a higher electrical resistivity compared to the Cu, Au, and Pt materials. Thus, it is expected that the Cr material provides lower shunt currents. In addition, the Cr element is known as exchange and coercive field decreasing material, which is useful to increase the PHE sensor sensitivity in trilayer structures [19–21]. In this study, we first provide a theoretical background that explains the PHE-based magnetic field sensor's output voltage and its sensitivity dependence on exchange bias. In the experimental part, we fabricate trilayer structures of NiFe (10 nm)/Cr (t_{Cr})/ IrMn (20 nm) where the t_{Cr} is varied between 0.0 nm and 1.0 nm with a 0.1 nm steps. The magnetic properties (EB field and coercive field) of sensor structures are investigated by recording the anisotropic magnetoresistance (AMR) signals under a magnetic field applied along the easy axis. Then the PHE sensor characteristics are determined as a function of Cr spacer layer thickness. In order to characterize sensor responses to external magnetic fields, a time-dependent experiment is carried out under positive and negative polarities of applied magnetic field.

2. Theoretical background

2.1. AMR and PHE signals

The planar Hall effect originating from anisotropic magnetoresistance (AMR) can be observed in ferromagnetic (FM) materials [22–24]. By using a six-terminal Hall bar geometry and assuming a single domain magnetization states of an in-plane magnetic anisotropy (Figure 1a), the following AMR voltage (V_{AMR}) response can be observed from the longitudinal terminals as a function of angle (φ) between magnetization ($\mathbf{M}$) and current (i_x) [25]:

$$V_{AMR}=\frac{i_x l}{wt}[\rho_\perp+(\rho_\parallel-\rho_\perp)\cos^2\varphi] \qquad (1)$$

where l is the length between longitudinal voltage terminals, w is the width, and t is the thickness of FM material (Figure 1a). $\rho_\parallel$ and $\rho_\perp$ are the resistivities which are measurable when the magnetization ($\mathbf{M}$) and current (i_x) are parallel ($\varphi = 0°$and $180°$) and perpendicular ($\varphi = 90°$and $270°$) to each other, respectively. It is known in the literature that $\rho_\parallel$ is bigger than $\rho_\perp$ for the ferromagnetic materials [25]. Therefore, V_{AMR} provides a maximum voltage when the magnetization is parallel to the applied current. As the magnetization rotates toward a perpendicular state, V_{AMR} approaches to a minimum as a function of $\cos^2\varphi$.

Besides, the transverse voltage of the same Hall bar geometry provides the following PHE voltage (V_{PHE}) response depending on φ [26]:

$$V_{PHE}=i_x\frac{(\rho_\parallel-\rho_\perp)}{t_{FM}}\sin\varphi\cos\varphi \qquad (2)$$

Due to the $\sin\varphi\cos\varphi$ dependence of V_{PHE} given in Equation (2), a maximum voltage is observed when the magnetization angle is $\varphi = 45°$ and $225°$, and it gives minimum for the $\varphi = 135°$ and $315°$.

It is important to mention here that the V_{AMR} depends on length (l) and width (w) of a Hall bar while the V_{PHE} is independent of them. This unique property of PHE-based sensors makes their fabrication in various sizes possible. Furthermore, the V_{PHE} is not sensitive to small temperature fluctuations [27]. Therefore,

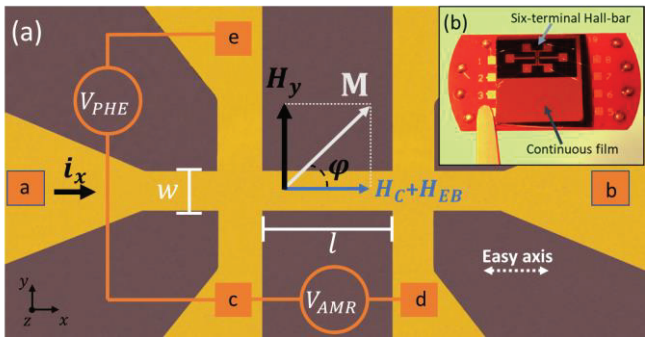

Figure 1. (a) A microscopic image of the six-terminal Hall bar geometry. Here, the constant dc current of i_x is applied between a-b terminals. The AMR voltage V_{AMR} is measured from the longitudinal c-d terminals, and the PHE voltage (V_{PHE}) is measured from transverse c-e terminals. The angle between magnetization (M) and applied current (i_x) is defined by φ. The effective magnetic anisotropy $H_C + H_{EB}$ is directed to $+_x$ direction. (b) A photograph of the fabricated sample mounted on a printed circuit board where the Hall bar and continuous film parts were simultaneously deposited.

PHE signal exhibits a higher signal-to-noise ratio (SNR) compared to the longitudinal AMR signal. Thus, the PHE provides a better magnetic field resolution which is defined by the lowest magnetic field that a sensor can recognize.

In addition, because of the V_{AMR} and V_{PHE} expressions given in Equations (1) and (2) are a direct function of magnetization angle (φ), these two signals can exhibit coherent behaviors with the magnetic hysteresis loops. Thus, the AMR and PHE signals can also be used for determining the exchange bias field (H_{EB}) and coercive field (H_C) values of a magnetic hysteresis loop obtained along the easy axis (see Figure 3).

3. PHE-based sensor design and its response to applied magnetic field

Figure 1a presents a microscopic image for the traditional cross-junction geometry of a PHE-based sensor with a coordinate system. Here the easy axis anisotropy field (H_C) of FM sensing layer is usually adjusted parallel to the current (i_x) path, and a magnetic field (H_y) is applied along the y-axis.

Before moving on to the explanation of PHE sensor response to applied magnetic field (H_y), it is important to mention here that, for the zero magnetic field, the magnetization is controlled by the easy axis magnetic anisotropy. Thus, M is free to stay initially along the easy axis either positive ($\varphi = 0°$) or negative ($\varphi = 180°$) x-directions when a single FM layer is used (without exchange bias). This results in a double PHE signal output during a magnetization reversal process as shown in the inset of Figure 2 [27]. The double signal is unwanted in many PHE sensor applications. In order to remove one of the PHE signals, the FM sensing layer can be exchange-biased either by using an antiferromagnetic layer or by using another FM layer with higher magnetic anisotropy that results in a unidirectional magnetic anisotropy in the FM sensing layer. Besides, to provide a higher magnetic anisotropy in the second FM layer, it can also be pinned by using an antiferromagnetic layer (FM/NM/FM/AFM). Because the unidirectional magnetic anisotropy pins the magnetic moments of FM sensing layer in one preferred direction (+x direction in our design), every time under zero field case, M rotates to its initial orientation (for example $\varphi = 0°$initially). Thus, a single PHE sensor response can be obtained as shown in Figure 2. In the exchange bias case, the magnetic moments of FM sensing material feel an additional unidirectional anisotropy field (H_{EB}) which is also defined toward +x direction in Figure 1a. Therefore, the effective anisotropy field that the magnetic moments in the FM layer feels can be assumed as $H_C + H_{EB}$.

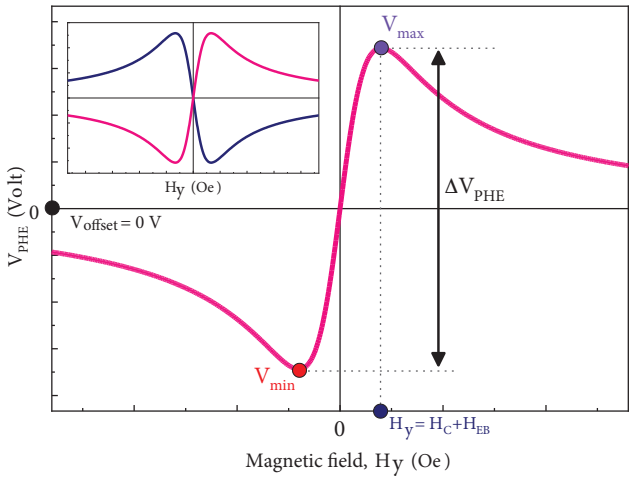

Figure 2. A traditional magnetic field (H_y) profile of a PHE sensor fabricated in a cross-junction geometry with an exchange-biased FM material (FM/AFM bilayer or FM/NM/AFM trilayer or FM/NM/FM/AFM spin-valve). The inset figure shows a schematic of the double magnetic field (H_y) profile of the PHE signal that can be obtained from a single FM material without exchange bias.

For the given configuration of PHE-based sensors in Figure 1a, Figure 2 shows a characteristic sensor signal as a function of H_y. When the H_y is very small compared to the $H_C + H_{EB}$, the PHE signal provides a quite linear region with a zero-offset. At this condition, magnetization ($\mathbf{M}$) exhibits a small rotation toward the applied magnetic field (H_y). By using the vector diagram presented in Figure 1a, the following approximation can be applied to determine the magnetization angle (φ) [26]:

$$\varphi \approx \frac{H_y}{H_C + H_{EB}} \tag{3}$$

Furthermore, because the φ is very small for this condition, $\sin\varphi \approx \varphi$ and $\cos\varphi \approx 1$ can be written. Thus, the following V_{PHE} expression can be obtained by replacing the $\sin\varphi\cos\varphi$ term into Equation (2):

$$V_{PHE} = \frac{i_x}{t}(\rho_{\parallel} - \rho_{\perp})\frac{H_y}{H_C + H_{EB}} \tag{4}$$

Besides, the magnetic field sensitivity (S) of a PHE sensor for the given cross-junction geometry can be determined by the following expression [24]:

$$S = \frac{V_{PHE}}{i_x H_y} \tag{5}$$

By using the approximation given in Equation (3), the following expression can also be written for sensor's magnetic field sensitivity (S):

$$S = \frac{1}{t}(\rho_{\parallel} - \rho_{\perp})\frac{1}{H_C + H_{EB}} \tag{6}$$

Equation 6 clearly indicates that the PHE sensor's magnetic field sensitivity is directly related to resistivity difference ($\rho_{\parallel} - \rho_{\perp}$) of FM material and magnitude of anisotropy terms ($H_C + H_{EB}$).

PHE sensitivity (S) is a very important parameter for sensor applications. In order to increase the S given in Equation (6), the exchange bias field (H_{EB}) can be minimized. This can be achieved via either increasing the thickness of the FM layer in bilayers [14] or inserting a nonmagnetic (NM) third layer between the FM and AFM layers (FM/NM/AFM) [8,12,16]. However, in the trilayer structures, when the electrical resistivity of the NM spacer layer is very low, a considerable decrease of V_{PHE} is observed (Figure 2). Therefore, although the addition of the NM spacer layer decreases the H_{EB}, an increase in sensor sensitivity may not be observed when the NM spacer layer thickness is increased [16]. For this reason, a proper choice of NM spacer layer is very important while designing a PHE sensor structure. Furthermore, the same shunting effect can be observed for the spin-valve structures (FM/NM/FM/AFM) due to an additional FM layer. It is very well known in the literature that the trilayer PHE sensor structure provides higher sensor sensitivity compared to bilayers and spin-valves [8].

3.1. Sensor fabrication and experimental details

The six-terminal Hall bar (cross-junction) geometry of the PHE sensor and continuous film parts were simultaneously fabricated on the same Si/SiO_2 (500 nm) substrates by the lift-off a trilayer structure as shown in Figure 1b. Here, the cross width (w) was 25 μm $\times$25 μm and the length (l) between longitudinal terminals was 100 μm. By using a magnetron sputtering system, $Ni_{80}Fe_{20}$ (10 nm), Cr (t_{Cr}), and $Ir_{22}Mn_{78}$ (20 nm) layers were sequentially deposited at room temperature. The nominal thickness of the Cr spacer layer was varied between 0 and 1 nm with a step of 0.1 nm. At the top of the sensor stack, a 3 nm thick Pt cap layer was used to avoid oxidation. During the sputtering process, Ar pressure was kept 5 $\times 10^{-3}$ mbar with a 20 sccm flow rate, and the dc powers applied to targets were 10 W, 10 W, 20 W, and 10 W, respectively. The easy axes of the PHE sensors have been aligned parallel to the current path via growth-induced magnetic anisotropy. For the electronic transport experiments, we used a home-made transport system [28–30]. Here we applied 1 mA dc current along the x-axis by using a Keithley 2400 sourcemeter, and we recorded the AMR and PHE voltages with a Keithley 2182a nanovoltmeter from longitudinal and transverse terminals, respectively. The H_C and H_{EB} values of PHE sensor structures were determined by the analysis of AMR data taken as a function of magnetic field swept along the easy axis (x-axis). In order to observe the PHE sensor characteristics, the magnetic field was swept along the hard axis (y-axis) and transverse voltages were recorded as described in the theoretical background. All the measurements were done at room temperature (T = 300 K).

4. Results and discussion

Magnetic properties (H_C and H_{EB}) for the PHE sensor structures of NiFe (10)/Cr (t_{Cr})/IrMn (20) (nm) were determined by recording AMR voltages with a 2 Oe magnetic field steps. Figure 3 presents an example for easy axis (H // i_x) measurements of hysteresis (MOKE) and AMR loops taken by using a bilayer structure of SiO_2/NiFe (10 nm)/IrMn (8 nm)/Pt (3nm). As indicated in the figure, during the magnetization switching process, the MOKE and AMR signals changed coherently. Here, the AMR signal provides deep points at the switching fields. By using these deep points, we determined H_C and H_{EB} values as 108 Oe and 81 Oe, respectively. When the 8 nm thick IrMn layer was used, H_C was bigger than H_{EB}. However, when we increased the thickness of IrMn in NiFe/IrMn bilayer structure from 8 to 20 nm, the hysteresis loop completely shifted to the left side. In this case, we determined H_{EB} = 124 Oe and H_C = 82 Oe (where $H_{EB} > H_C$) as shown in Figure 4. This structure was better to investigate the effect of Cr spacer layer compared to 8 nm

IrMn structure. As we inserted a Cr spacer layer up to 1 nm between the NiFe (10 nm) and IrMn (20 nm) layers, H_{EB} and H_C values decreased monotonically to 20 Oe and 37 Oe, respectively. Interestingly, the H_{EB} exhibited a faster decrease compared to the H_C with the increasing t_{Cr}. Thus, when the t_{Cr} was above 0.4 nm, again H_C was bigger than H_{EB}. This fast decrease in H_{EB} is very beneficial for PHE sensors since the thinner Cr layer provides lower shunt current as mentioned in the theoretical background.

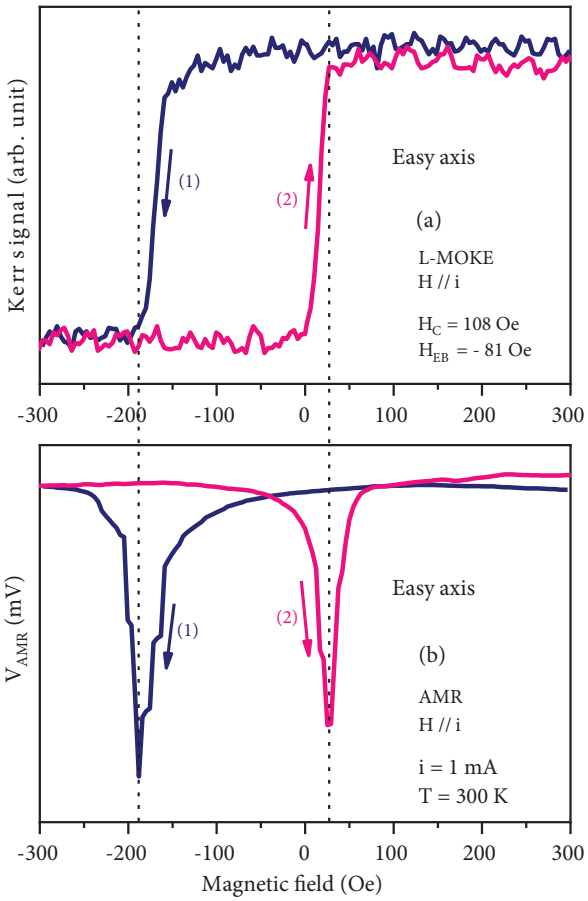

Figure 3. (a) An easy axis magnetic hysteresis loop (by MOKE signal) and (b) an AMR voltage change (by electrical transport) obtained from the NiFe (10 nm)/IrMn (8 nm) bilayer structure. (1) indicates the data recorded during magnetic field sweep from positive to negative while (2) shows from negative to positive. The magnetic hysteresis loop and AMR signal exhibited a coherent behavior as a function of applied magnetic field. Thus, the H_{EB} = 81 Oe and H_C = 108 Oe values can be determined from the deep points of AMR signal.

Figure 5a presents the magnetic field profiles of PHE sensor signals obtained from the NiFe (10 nm)/IrMn (20 nm) bilayer and the NiFe (10 nm)/Cr (1 nm)/IrMn (20 nm) trilayer structures. Here, insertion of the Cr spacer layer provides mainly two effects on PHE signal. One is the reduction of both H_{EB} and H_C. Thus, the maximum and minimum peak positions observed in these signals shifted to a lower magnitude of magnetic field. The other effect is a reduction of ΔV_{PHE} due to the increased shunt current. The ΔV_{PHE} was decreased from 185 μV to 165 μV. Although the ΔV_{PHE} was decreased, the fast decrease in H_{EB} increased the slope of linear region which is described as sensor's magnetic field sensitivity (S) [see Equation (6)]. The magnetic field sensitivities of PHE sensors determined from the linear regions of PHE signals are presented in Figure 5b as a

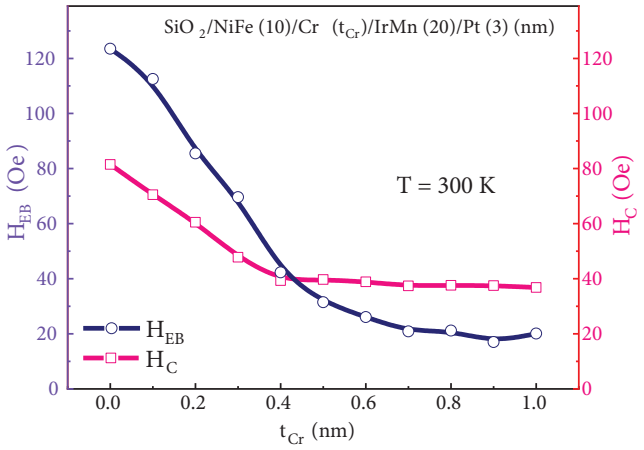

Figure 4. The change in the exchange bias (H_{EB}, open circles) and coercive field (H_C, open squares) as a function of Cr spacer layer thickness (t_{Cr}). The solid lines are guides for the eye.

function of Cr spacer layer thickness. The bilayer structure of the PHE sensor made in cross-junction geometry provided $S = 0.86$ μV/(Oe·mA) magnetic field sensitivity. This value of sensitivity is very similar to that of a previous study with a Pt spacer layer [12]. As the thickness of Cr spacer layer increased up to 0.7 nm, the sensitivity monotonically increased a maximum 4.4 μV/(Oe·mA). Above this thickness, the sensitivity slightly decreased to 4.3 μV/(Oe·mA). In addition, during the positive and negative magnetic field sweeping, the PHE signals did not coincide with each other. The double signal characteristic given in Figure 5a is different from the data presented in the inset of Figure 2, and the following three different contributions can explain this double signal behavior. (i) To apply an external magnetic field, we used an electromagnet that has a metallic core. The remanence magnetization occurred in this core can provide a different magnetic field magnitude during electromagnet current sweeping. Therefore, the magnetic field that the PHE sensor feels during the positive and negative current sweeping is different. This gives a double PHE signal. If a Helmholtz coil is used, this contribution can be eliminated. (ii) While recording the PHE voltages by using a Keithley 2182a, the filtering (averaging) effect can cause a delayed response if the time for recording per data is too short. This delayed response can be minimized by increasing the recording time. (iii) In the literature, it is also known that the incoherent rotation of magnetization in the FM sensing layer can provide a double characteristic in PHE signal during field sweeping [12,16,31].

In order to show stable sensor responses to positive and negative magnetic fields, time-dependent measurements were carried out by using the NiFe(10 nm)/Cr (0.7 nm)/IrMn (20) nm sensor structure (Figure 6). The time profile of the PHE signal was obtained by continuously recording the sensor voltage (V_{PHE}). In the first step, the V_{PHE} was recorded under zero magnetic field and this voltage was set as 0 V (reference). For the second and third steps, a positive and negative 2 Oe magnetic field was applied along the y-axis and removed for 250 s, respectively. Lastly, all of these steps were repeated two more times. The data presented in Figure 6 indicates that the fabricated PHE sensor is very sensitive to the polarity and magnitude of the applied magnetic fields. For the $\pm$2 Oe magnetic fields, the V_{PHE} exhibited $\pm$12 μV voltage change. As clearly seen, the sensor responses are very stable and quite symmetric when the experiment steps are repeated. Besides, $\pm$100 nV noise level of PHE sensor signal provides a 1.6 μT magnetic field resolution for 1 mA sensor current. This resolution can be enhanced by increasing the sensor current (i_x) and reducing the sensor's noise levels [32].

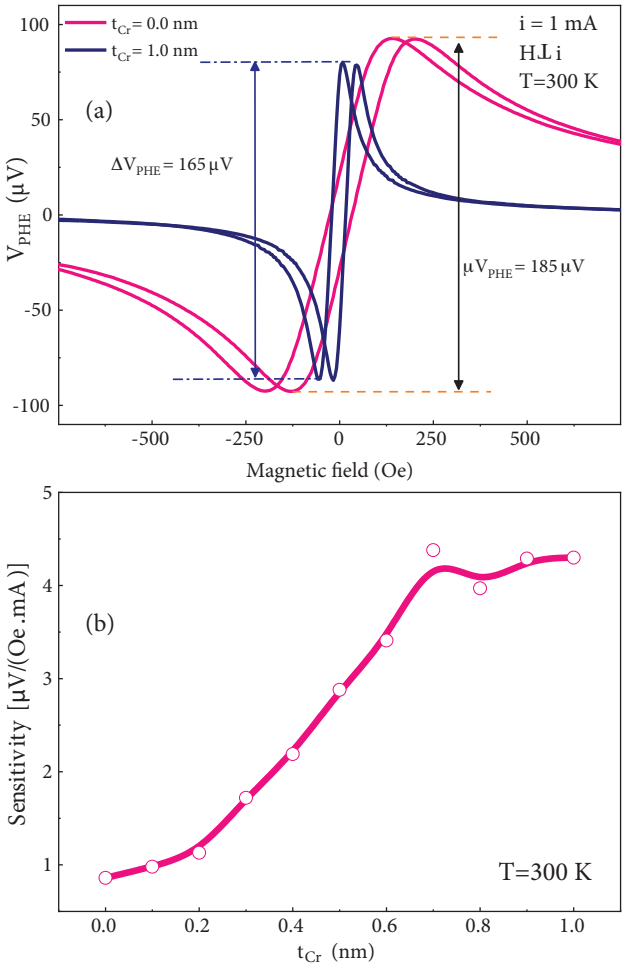

Figure 5. (a) The magnetic field profiles obtained from the PHE sensors fabricated with a bilayer NiFe(10 nm)/ IrMn (20 nm) and trilayer NiFe (10 nm)/ Cr (1 nm)/IrMn (20 nm) structures. (b) The change in the magnetic field sensitivity as a function of Cr spacer layer thickness (t_{Cr}).

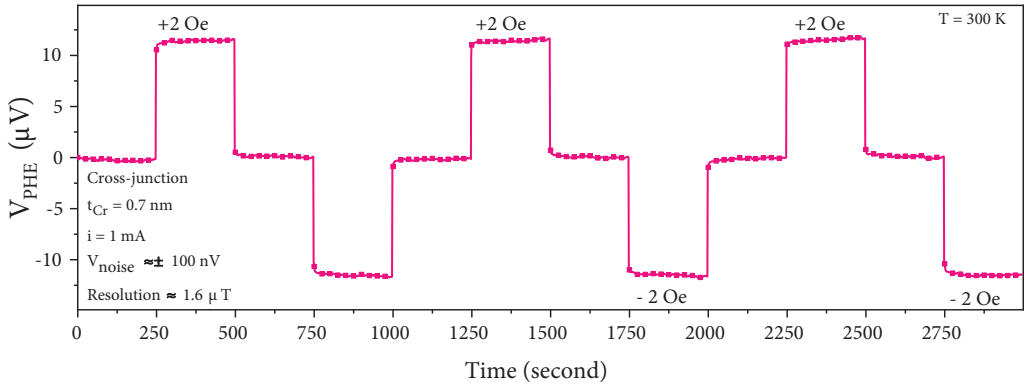

Figure 6. Time profile for the PHE sensor structure fabricated with a 0.7 nm thick Cr spacer layer. The data shows that the sensor states are quite stable and repeatable under positive and negative polarities of the magnetic field. Besides, the PHE signal of investigated cross-junction has a ±100 nV noise level for 1 mA sensor current.

5. Conclusion

We performed a systematic study on tuning the PHE sensor sensitivity and exchange bias via inserting a Cr spacer layer between the NiFe (10 nm) and IrMn (20 nm) layers. When the Cr thickness was increased up to 1 nm with a step of 0.1 nm, we observed a fast decrease in H_{EB}, which results in an enhancement of PHE sensitivity. The fast decreasing in H_{EB} can be useful to decrease shunt currents. Besides, a maximum sensitivity of 4.4 μV/(Oe·mA) was observed for the 0.7 nm thick Cr spacer layer. Time-dependent experiments revealed that the fabricated PHE sensors are very sensitive to polarity and magnitude of magnetic fields applied along the y-axis. We observed quite stable and repeatable sensors states. These results indicate that Cr-spacer-based PHE sensors are promising for future sensor applications that require a low magnetic field sensing.

Acknowledgment

This work was supported by TÜBİTAK (The Scientific and Technological Research Council of Turkey) through the project number 116F083.

References

[1] Kim S, Torati SR, Talantsev A, Jeon C, Lee S, Kim C. Performance validation of a planar hall resistance biosensor through beta-amyloid biomarker. Sensors 2020; 20: 434. doi: 10.3390/s20020434

[2] Hansen MF, Rizzi G. Exchange-biased AMR bridges for bagnetic field sensing and biosensing. IEEE Transactions on Magnetics 2017; 53 (4): 4000211. doi: 10.1109/TMAG.2016.2614012

[3] Østerberg FW, Rizzi G, Donolato M, Bejhed RS, Mezger A et al. On-chip detection of rolling circle amplified DNA molecules from bacillus globigii spores and vibrio cholerae. Small 2014; 10 (14): 2877. doi: 10.1002/smll.201303325

[4] Volmer M, Avram M. On designing a positioning and detection system for a lab-on-a-chip device. Romanian Journal of Information Science and Technology 2010; 13 (4): 378-388.

[5] Oh S, Jung Y, Kim S, Kim S, Hu X et al. Remote tactile sensing system integrated with magnetic synapse. Scientific Reports 2017; 7:16963. doi: 10.1038/s41598-017-17277-2

[6] Montaigne F, Schuhl A, Van Dau FN, Encinas A. Development of magnetoresistive sensors based on planar Hall effect for applications to microcompass. Sensors and Actuators A: Physical 2000; 81: 324-327. doi: 10.1016/S0924-4247(99)00102-8

[7] Pham HQ, Tran BV, Doan DT, Le VS, Pham QN et al. Highly Sensitive Planar Hall Magnetoresistive Sensor for Magnetic Flux Leakage Pipeline Inspection. IEEE Transactions on Magnetics 2018; 54 (6): 6201105. doi: 10.1109/TMAG.2018.2816075

[8] Hung TQ, Oh S, Sinha B, Jeong JR, Kim DY, Kim C. High field-sensitivity planar Hall sensor based on NiFe/Cu/IrMn trilayer structure. Journal of Applied Physics 2010; 107 (9): 09E715. doi: 10.1063/1.3337739

[9] Hung TQ, Jeong JR, Kim DY, Duc NH, Kim C. Hybrid planar Hall-magnetoresistance sensor based on tilted cross-junction. Journal of Physics D: Applied Physics 2009; 42: 055007. doi: 10.1088/0022-3727/42/5/055007

[10] Oh S, Patil PB, Hung TQ, Lim B, Takahashi M et al. Hybrid AMR/PHR ring sensor. Solid State Communications 2011; 151 (18): 1248-1251. doi: 10.1016/j.ssc.2011.05.049

[11] Henriksen AD, Dalslet BT, Skieller DH, Lee KH, Okkels F, Hansen MF. Planar Hall effect bridge magnetic field sensors. Applied Physics Letters 2010; 97 (1): 013507. doi: 10.1063/1.3460290

[12] Pişkin H, Akdoğan N. Interface-induced enhancement of sensitivity in NiFe/Pt/IrMn-based planar hall sensors with nanoTesla resolution. Sensors and Actuators A: Physical 2019; 292: 24-29. doi: 10.1016/j.sna.2019.04.003

[13] Thanh NT, Chun MG, Ha ND, Kim KY, Kim CO, Kim CG. Thickness dependence of exchange anisotropy in NiFe/IrMn bilayers studied by Planar Hall Effect. Journal of Magnetism and Magnetic Materials 2006; 305 (2): 432-435. doi: 10.1016/j.jmmm.2006.01.228

[14] Damsgaard CD, Freitas SC, Freitas PP, Hansen MF. Exchange-biased planar Hall effect sensor optimized for biosensor applications. Journal of Applied Physics 2008; 103(7): 07A302. doi: 10.1063/1.2830008

[15] Özer B, Pişkin H, Akdoğan N. Shapeable planar Hall sensor with a stable sensitivity under concave and convex bending. IEEE Sensors Journal 2019; 19: 5493-5498. doi: 10.1109/JSEN.2019.2907616

[16] Li XJ, Feng C, Chen X, Zhang JY, Liu YW et al. Enhanced planar hall sensitivity with better thermal stability by introducing interfacial modification of Au spacer. Journal of Magnetism and Magnetic Materials 2015; 381:386-389. doi: 10.1016/j.jmmm.2015.01.022

[17] Thanh NT, Kim KW, Kim CO, Shin KH, Kim CG. Microbeads detection using Planar Hall effect in spin-valve structure. Journal of Magnetism and Magnetic Materials 2007; 316: 238. doi: 10.1016/j.jmmm.2007.02.100

[18] Tu BD, Cuong LV, Hung TQ, Giang DTH, Danh TM et al. Optimization of spin-valve structure NiFe/Cu/NiFe/IrMn for planar Hall effect based biochips. IEEE Transactions on Magnetics 2009; 45: 2378-2382. doi: 10.1109/TMAG.2009.2018580

[19] Tafur M, Alayo W, Xing YT, Baggio-Saitovitch E, Nascimento VP. Long-range interaction and induced spin polarization in the spacer of the NiO/Cu/NiFe and NiO/Cr/NiFe trilayers. Journal of Physics D: Applied Physics 2009; 42: 135001. doi: 10.1088/0022-3727/42/13/135001

[20] Yanson Y, Petracic O, Westerholt K, Zabel H. Tuning the exchange bias by using Cr interfacial dusting layers. Physical Review B 2008; 78 (20): 205430. doi: 10.1103/PhysRevB.78.205430

[21] Akdoğan N, Yağmur A, Öztürk M, Demirci E, Öztürk O, Erkovan M. Interface induced manipulation of perpendicular exchange bias in Pt/Co/(Pt,Cr)/CoO thin films. Journal of Magnetism and Magnetic Materials 2015; 373: 120-123. doi: 10.1016/j.jmmm.2014.03.036

[22] Ky V-D. Plane Hall effect in ferromagnetic metals. Journal of Experimental and Theoretical Physics 1966; 23: 809-813.

[23] Ky V-D. Planar Hall effect in ferromagnetic films. Physica Status Solidi 1968; 26: 565-569.

[24] Schuhl A, Van Dau FN, Childress JR. Low-field magnetic sensors based on the planar Hall effect. Applied Physics Letters 1995; 66 (20): 2751. doi: 10.1063/1.113697

[25] Mcguire TR, Potter RI. Anisotropic Magnetoresistance in Ferromagnetic 3D Alloys. IEEE Transactions on Magnetics 1975; 11: 1018. doi: 10.1109/TMAG.1975.1058782

[26] Ejsing L, Hansen MF, Menon AK, Ferreira HA, Graham DL, Freitas PP. Planar hall effect sensor for magnetic micro- and nano bead detection. Applied Physics Letters 2004; 84 (23): 4729. doi: 10.1063/1.1759380

[27] Van Dau FN, Schuhl A, Childress J, Sussiau M. Magnetic sensors for nanotesla detection using planar Hall effect. Sensors and Actuators A: Physical 1996; 53: 256-260. doi: 10.1016/0924-4247(96)01152-1

[28] Demirci E, Akdoğan N. Multifunctional sample holder and high resolution detection system for magneto-optical Kerr effect measurements. TR Patent 2015 09249 B (21 June 2019).

[29] Akdoğan N, Öztürk M, Erdem D. Liquid nitrogen and liquid helium flow measurement chamber with optical window. TR Patent 2015 17168 B (21 November 2018).

[30] Demirci E. Investigation of perpendicular exchange bias effect in magnetoelectric Cr_2O_3 based thin films, PhD Thesis, Gebze Technical University, Department of Physics, 2016.

[31] Sinha B, Hung TQ, Ramulu TS, Oh S, Kim K et al. Planar Hall resistance ring sensor based on NiFe/Cu/IrMn trilayer structure. Journal of Applied Physics 2013; 113: 063903. doi: 10.1063/1.4790139

[32] Nhalil H, Givon T, Das PT, Hasidim N, Mor V et al. Planar Hall Effect Magnetometer With 5 pT Resolution. IEEE Sensors Letters 2019; 3 (12): 2501904. doi: 10.1109/LSENS.2019.2947681